Kalman filter and Neural Network methods for detecting irregular variations of TEC around the time of powerful Mexico (M$_w$=8.2) earthquake of September 08, 2017

Akhoondzadeh Hanzaei, M.*

Assistant Professor, Department of Remote Sensing, School of Surveying and Geospatial Engineering, College of Engineering, University of Tehran, Iran

Abstract

In 98 km SW of Tres Picos in Mexico (15.022° N, 93.899° W, 47.40 km depth) a powerful earthquake of M$_w$=8.2 took place at 04:49:19 UTC (LT=UTC-05:00) on September 8, 2017. In this study, using three standard, classical and intelligent methods including median, Kalman filter, and Neural Network, respectively, the GPS Total Electron Content (TEC) measurements of three months were surveyed to detect the potential unusual variations around the time and location of Mexico earthquake. Every three implemented methods indicated a striking irregular variation of TEC at the earthquake time. However, on the earthquake day, the geomagnetic indices D$_{st}$ and A$_p$ have exceeded the allowed ranges and even reached maximum values during the studied time period. Besides, the solar index of F10.7 showed high activity around the earthquake day. Therefore, it is difficult to acknowledge the seismicity nature of the detected TEC unusual variations on earthquake day. Therefore, in this case, we encounter a mixed and complex behavior of ionosphere.

Keywords: Earthquake Precursor, Ionosphere, Geomagnetic activity, GPS, Mexico earthquake, TEC.

1. Introduction

The preseismic unusual variations in lithosphere, atmosphere, and ionosphere without significant man-made, seasonal, solar and geomagnetic disturbances may be considered as earthquake precursors (Pulinets and Boyarchuk, 2004). It should be noted that statistical analysis and evaluation of different earthquake precursors in different case studies are necessary for development of precursor's studies. The ionospheric irregular variations can be observed in the D, E and F layers, 1 to 10 days before the earthquakes and continue a few days after them. Fortunately, there are many scientific reports on satellite surveying of the ionospheric plasma and measuring its parameters including electron and ion density and temperature, electric potential and electromagnetic fields in different frequency channels associated with seismic activities (Parrot, 1995; Liu et al., 2004; Hayakawa and Molchanov, 2002; Pulinets and Boyarchuk, 2004; Akhoondzadeh, 2011).

Contrary to methods that suppose the Earth's crust to have an ideal homogeneous structure and disregard the physical and chemical changes occurring inside the earth, there exist hypotheses explaining the seismoelectromagnetic mechanism based on geophysical and geochemical processes:

- Direct wave production in a wide band spectrum by compression of rocks close to earthquake epicenter could be likely related to piezo-electric and tribo-electric effects (Pulinets and Boyarchuk, 2004);
- Rising fluids under the ground would lead to the emanation of warm gases (Pulinets, 2009);
- Activation of positive holes that can reach the ground surface (Freund, 2009);
- Emissions of radioactive gas or metallic ions such as radon that increase the Earth surface potential (Pulinets, 2009).

Pre-seismic electric field and its polarity cause the electrons in the F-layer to penetrate to lower layers and therefore to create an anomaly in the ionospheric parameters (Pulinets, 2009). The presence of ions and charge separation lead to the generation of the strong electric field, which penetrates into the ionosphere and creates seismo-ionospheric effects. The vertical electric field on the ground surface is transformed into an electric field perpendicular to the geomagnetic field lines. This zonal component leads to plasma density anomalies,

---

*Corresponding author: makhonz@ut.ac.ir

which are observed in the earthquake area. (Parrot, 1995; Hayakawa and Molchanov, 2002; Pulinets and Ouzounov, 2011; Sorokin and Pokhotelov, 2014). In the vicinity of the equatorial anomaly, a zonal component can be generated using the mechanism proposed in Pulinets (2009).

Nowadays, GPS Total Electron Content (TEC) measurements are very effective tools to survey the ionosphere over the regions supported by the GPS receivers. Liu et al. (2004) statistically described the temporal parameters of the seismo-ionospheric precursors detected during 1-5 days prior to the earthquakes using TEC data for 20 major earthquakes in Taiwan. Klimenko et al. (2012) applied numerical calculations to check the proposed mechanism of the pre-seismic TEC anomalies formation under the influence of additional zonal electric field. Namgaladze et al. (2013) presented the results of a study of the abnormal variations in the TEC of the ionosphere observed before the earthquake of January 12, 2010, in Haiti. They showed the prevalence of increased TEC values (positive disturbances), neighboring negative disturbances of lower magnitudes, localization, magnetic conjugacy of high-intensity effects in the Southern Hemisphere, and disappearance of disturbances around midday. This paper is dedicated to evaluating the effectiveness of GPS-TEC measurements to detect the ionospheric irregular variations around the time of the powerful Mexico earthquake.

2. The implemented methods

There are many classical and intelligent methods to detect the unusual variations in a nonlinear time series (Akhoondzadeh, 2012; 2013). In this study, in addition to the median method, other methods including Kalman filter and Neural Network (NN) as classical and intelligent methods, respectively, are implemented to detect the irregular variations.

2.1. Median

Daily variations of the ionosphere depend on season, geographic location, thermospheric winds, traveling ionospheric disturbances and other unknown parameters. The unknown variations preclude using methods based on the normal distribution of data. As the fluctuation of the ionospheric parameters

does not often follow a Gaussian probability function, some researchers (Liu et al., 2004; Pulinets and Boyarchuk, 2004) used the median value and the interquartile range of data to specify higher and lower bounds in order to distinguish seismic anomalies from the background variations. The interquartile range (IQR) is a measure of variability, based on dividing a data set into quartiles. Quartiles divide a rank-ordered data set into four equal parts. The values that divide each part are called the first, the second, and the third quartiles; and they are denoted by Q1, Q2, and Q3, respectively.

- Q1 is the "middle" value in the first half of the rank-ordered data set.
- Q2 is the median value in the set.
- Q3 is the "middle" value in the second half of the rank-ordered data set.

The interquartile range is equal to Q3 minus Q1.

The higher and lower bounds of the mentioned range can be calculated using the following equations:

$$x_{high} = M + k \times IQR \tag{1}$$

$$x_{low} = M - k \times IQR \tag{2}$$

$$x_{low} < x < x_{high} \Rightarrow -k < \frac{x-M}{IQR} < k;$$
$$Dx = \frac{x-M}{IQR} \tag{3}$$

where x, x_{high}, x_{low}, M, IQR and Dx are parameter (Here, TEC), higher bound, lower bound, median value, interquartile range and differential of x, respectively. For a given x, values of M and IQR have been calculated for the whole period of interest for any interval of 1 hour. According to Equation (3), $p = \pm 100 \times (|Dx| - k)/k$ indicates the percentage of parameter change from the undisturbed state. If an observed TEC falls out of either the associated lower or higher bound, it is concluded with a confidence level of about 80-85% that a lower or higher irregular value is detected (Liu et al., 2004).

2-2. Kalman filter

Kalman filter is a recursive solution to optimize the described systems in the state space. This filter is a set of mathematical

equations to optimize prediction equations using an estimation of state variables and minimization of error covariance. It is suitable for the stationary as well as dynamic and linear processes, and it can be applied to non-linear systems using Taylor expansion equations. The filter has high capabilities in the determination of inner variables and simultaneously solves the state and measurement equations in order to reach optimized unobservable states. In other words, this method uses observed variables ($y_1, y_2,..., y_t$) to estimate state (x_i) with minimum error. If *i=t, i>t* or *i<t*, this method is known as filtering, prediction or interpolation respectively. Equations (4) and (5) are state and measurement equations (Haykin, 2001):

$$x_{t+1} = Fx_t + w_t \tag{4}$$

$$y_t = Hx_t + v_t \tag{5}$$

where w_t and v_t are white noise vectors (*P(w): N(0,Q) and P(v): N(0,R)*). *P* and *N* are probability distribution function and normal distribution function respectively. *Q* and *R* are standard deviation parameters. *F* is the transition matrix taking the state x_t from time *t* to time *t+1*. *H* is the measurement matrix. If x_t is supposed to be a real state at time *t*, then pre-estimation error ($e_t^- = x_t - \hat{x}_t^-$), post-estimation error ($e_t^+ = x_t - \hat{x}_t^+$), pre-error covariance ($p_t^- = E(e_t^- e_t^{'-})$) and post-error covariance ($p_t^+ = E(e_t^+ e_t^{'+})$) can be defined.

The main aim in the Kalman filter is an estimation of $\hat{x}_t^+$ (post-estimation of state) using linear integration of $\hat{x}_t^-$ (pre-estimation of state) and measured error ($y_t - H \hat{x}_t^-$) as Equation (6).

$$\hat{x}_t^+ = \hat{x}_t^- + k_t(y_t - H \hat{x}_t^-) \tag{6}$$

k_t is the Kalman coefficient and must be defined based on the minimum of post-error covariance (Equation 7).

$$k_t = p_k^- H^T (Hp_k^- H^T + R)^{-1} \tag{7}$$

Regarding the mentioned equations, measurements would be reliable when covariance of measurement error is close to zero. Kalman filter equations are classified into two categories: 1) time update; time retrieval equations update state and covariance matrices based on the pre-measurements (Equations 8 and 9), 2) measurement update; measurement retrieval equations for feedback of time update effects in the system and reach to optimum state based on the measurements (Equations 10, 11 and 12).

$$\hat{x}_t^- = F \hat{x}_{t-1}^+ \tag{8}$$

$$p_t^- = Fp_{t-1}F^T + Q \tag{9}$$

$$k_t = p_t^- H^T (Hp_t^- H^T + R)^{-1} \tag{10}$$

$$\hat{x}_t^+ = \hat{x}_t^- + k_t(y_t - H \hat{x}_t^-) \tag{11}$$

$$p_t = (1 - k_t H) p_t^- \tag{12}$$

Therefore, in the beginning, the prediction process is done, then it is corrected based on the observations and again prediction process is repeated. If however, the state and measurement equations are nonlinear (such as time series of earthquake precursors), they could be changed into linear equations using Taylor expansion called extended Kalman filter. This is one of the striking characteristics of Kalman filter. In order to detect irregular variation using Kalman filter, total available data are split into a training set and a test set. This method uses the observed variables ($y_1, y_2,..., y_t$) to estimate state (x_i) with minimum error. At the beginning, prediction process is done, then after the improvement of the Kalman filter parameters, it is corrected based on the observations and again prediction process is repeated. If the difference between the observed TEC value and the predicted TEC value is greater than a threshold value (i.e. $\mu \pm \sigma$; μ and σ are the mean and the standard deviation parameters, respectively), the observed TEC value in quiet geomagnetic (i.e. $Dst > -20\,nt$, $Dst < 20\,nt$, $Ap < 20$ and F10.7 <120) is regarded as

irregular variation (Akhoondazdeh, 2011).

2-3. Neural Networks

Artificial Neural Networks are a class of intelligent systems that can discover patterns with a few prior assumptions and learn any complex functional relationship from the data, to model a phenomenon. Neural networks are able to capture the autocorrelation structure in a time series even if the underlying law governing the series is unknown or too complex to describe.

In a notable number of scientific works, artificial neural networks have been proposed as a promising alternative approach to time series forecasting. A large number of successful applications have shown that neural networks can be a very effective tool in modeling and forecasting of nonlinear time series (Zhang, 2001).

An NN is made up of simple processing units, the neurons, which are connected in a network by a large number of weighted links where the acquired knowledge is stored.

An input x_j is transmitted through a connection, which multiplies its strength by a weight w_{ij} to give a product $x_j w_{ij}$. This product is an argument to a transfer function f, which yields an output represented as $y_i = f(x_j w_{ij})$ where i is an index of neurons in the hidden layer and j is an index of an input to the neural network (Paoli et al., 2010).

The most popular and successful model is the feed forward Multi-Layer Perceptron (MLP) network. In an MLP, neurons are grouped in layers and only forward connections exist.

In order to detect irregular variation, total available data are split into a training set and a test set. The training set is used for the construction of the neural network, whereas the test set is used for measuring the predictive error of the model. The training process is used essentially to find the connection weights of the networks (Pao, 2007). If the prediction error exceeds the pre-defined threshold, the measured value could be considered as an irregular variation.

In order to determine the best network configuration, the effective parameters, which influence the value of predictive error, including the number of pattern input; lag value: the number of hidden layer and their number of neurons; the activation functions and the learning algorithm have been

obtained via an iterative process to assess the minimum predictive error when the training process was implemented.

Concerning the activation function for the output layer, the best results were obtained with the linear function. The transfer function used for all hidden nodes is the tan-sigmoid function. The tan-sigmoid function is:

$$f(x) = \frac{2}{1 + e^{-2z}} - 1 \tag{13}$$

The well-known Levenberg–Marquardt optimization has been selected as training algorithm. To start the prediction process, N observations $y_1, y_2, \ldots, y_N$ are selected as the training set and the remaining ones $y_{N+1}, y_{N+2}, \ldots, y_{N+m}$ are considered as the test set. The number of input nodes p corresponds to the number of lagged observations used to discover the underlying pattern in a time series. Different input nodes can affect either the learning or predictive capability of the network (Pao, 2007). In this study, a network with three nodes in the input layer, two nodes in the hidden layer and one node in the output layer has been proposed. In other words, every four observations in the training set constitute a pattern vector, three of which are input values and the last one is the output value.

The training patterns in the proposed network are:

$X_4 = f(X_1, X_2, X_3)$
$X_5 = f(X_2, X_3, X_4)$
.
.
$X_N = f(X_{N-3}, X_{N-2}, X_{N-1})$

The training process is executed to find the optimized connection weights such that the prediction error (*PE*) is minimized. *PE* equation can be written as:

$$PE = \sum_{i=4}^{N} (X_i - \hat{X}_i) \tag{14}$$

where, $\hat{X}_i$ is the output of the network.

The testing patterns are,

$X_{N+4} = f(X_{N+1}, X_{N+2}, X_{N+3})$
$X_{N+5} = f(X_{N+2}, X_{N+3}, X_{N+4})$
.
.
$X_{N+m} = f(X_{N+m-3}, X_{N+m-2}, X_{N+m-1})$

For detection of irregular variations using the NN method, total available data are split into a training set and a test set. The training set is used to determine the weight and bias parameters of NN, whereas the test set is used for measuring the model prediction error. If the prediction error (difference value between the actual value and the predicted value), exceeds the limited bounds $\mu \pm \sigma$, (μ and σ are the mean and the standard deviation) the irregular variation is detected (Akhoondazdeh, 2013).

3. The used data
3-1. GPS-TEC Data
Recently, the extending network of GPS receivers has generated an increasing amount of data regarding the ionosphere state. TEC is the integrated number of the electrons within the block between the satellite and receiver or between two satellites. The GPS satellites transmit two frequencies of signals (f_1=1575.42 MHz and f_2=1227.60 MHz). The received signals in ground stations contain many effects such as ionospheric, tropospheric, hardware and random errors. The ionosphere is a dispersive medium and its effects can be evaluated with measurement of the modulations on the carrier phases recorded by dual-frequency receivers. To study TEC variations, data of Global Ionospheric Map (GIM) provided by NASA Jet Propulsion Laboratory (JPL) were used. The GIM is constructed into $5° \times 2.5°$ (Longitude, Latitude) grid with a time resolution of 1 hour. GIM data are generated on a daily basis using data from about 150 GPS sites of the International GNSS Service (IGS) and other institutions. Instrumental biases, so-called differential P1-P2 code biases (DCB), for all GPS satellites and ground stations are estimated as constant values for each day (Mannucci et al., 1998). To convert line-of-sight TEC into vertical TEC, a modified single-layer model mapping function approximating the JPL extended block model mapping function is adopted.

3-2. Space Weather (SW) and solar geomagnetic data
The ionospheric parameters are affected by SW phenomena including solar flares and CME, geomagnetic storms, especially in the equatorial and polar regions. Besides, auroral activity has an important role in the mid-latitude ionosphere perturbations. In other words, the ionosphere current and equatorial storm-time ring current in periods of solar-terrestrial interactions produce significant geomagnetic field disturbances observed on the ground. Accordingly, the measured ionospheric plasma parameters may display variations during and in absence of seismic activity. Therefore, it is difficult to separate pre-seismic ionospheric phenomena from the ionospheric disturbances due to the solar-terrestrial activities. Consequently, to distinguish the seismo-ionospheric perturbations from solar geomagnetic disturbances, the indices of D_{st}, Ap and F10.7 were checked. The detected irregular variations of TEC in quiet solar geomagnetic conditions may be associated with seismic activities. The A_p index monitors the planetary activity on a worldwide scale while the D_{st} index records the equatorial ring current variations (Mayaud, 1980). The F10.7 index represents a measure of diffuse, nonradiative heating of the coronal plasma trapped by magnetic fields over active regions, and is an excellent indicator of overall solar activity levels. The ionospheric effect caused by geomagnetic storm has a global impact being observed all over the world while the seismogenic effect is observed only by stations with distance less than 2000 km from the potential epicenter.

Figure 1 illustrates the variations of D_{st}, A_p and F10.7 indices, during the period of July 1 to September 30, 2017. An asterisk indicates the earthquake time. The X-axis represents the days relative to the earthquake day. The Y-axis represents the universal time coordinate.

The irregular D_{st} values are observed on earthquake day when this parameter exceeds the lower boundary value (i.e. -20 nT), reaching the lowest value of -142 and -128 nT at 02:00 and 03:00 UTC, respectively. Similar unusual variations are also seen at other times of earthquake date with the value of about -120 nT. The high geomagnetic activities are clearly observed on September 8, 2017, when the A_p value reach the maximum value of 236, between 13:00 and 14:00 UTC. The unusual variations of the A_p indices are also seen on earthquake day

between 02:00 and 03:00 UTC with the value of 207. This index shows the high geomagnetic activities on earthquake date. The F10.7 value gradually increases from about 14 days before the earthquake and reaches the maximum value of 182.50 SFU on September 4, 2017 (4 days before the event).

4. Case study

In 98 km SW of Tres Picos in Mexico (15.022° N, 93.899° W, 47.40 km depth) a strong earthquake of M_w=8.2 took place at 04:49:19 UTC (LT=UTC-05:00) on September 8, 2017 (https://earthquake.usgs.gov/). It was the second strongest earthquake recorded in the country's history, behind the magnitude 8.6 earthquake in 1787.

Figure 2(a) shows TEC variations derived from GIM data and the closest node (15° N, 95° W) to the epicenter during the period of July 1 to September 30, 2017. By visual inspection and without performing any special analysis, unusual TEC values are clearly seen around the earthquake day, especially between five days before the event to earthquake day. The TEC value reaches to a maximum value of 52.8 (TECU) on September 3, 2017 (five days before the earthquake) at 21:00 UTC. However, this sharp irregular variation cannot be considered as a seismo-ionospheric irregular variation because the geomagnetic activities are more than the allowed ranges at this time. After implementing the median method, Dx that will be called DTEC here is calculated using Equation (3).

Figure 2(b) shows variations of DTEC. The irregular variations are clearly seen between 02:00 and 06:00 UTC on earthquake day. DTEC reaches to a maximum value of 8.97 at 05:00 UTC that is the earthquake time. Figure 3 shows the time-series of variations of TEC, Dst, A_p, and F10.7 during the period of July 1 to September 30, 2017 at 05:00 UTC. It is seen that the mentioned parameters exceed the allowed boundaries (quiet geomagnetic conditions) on earthquake day at 05:00 UTC.
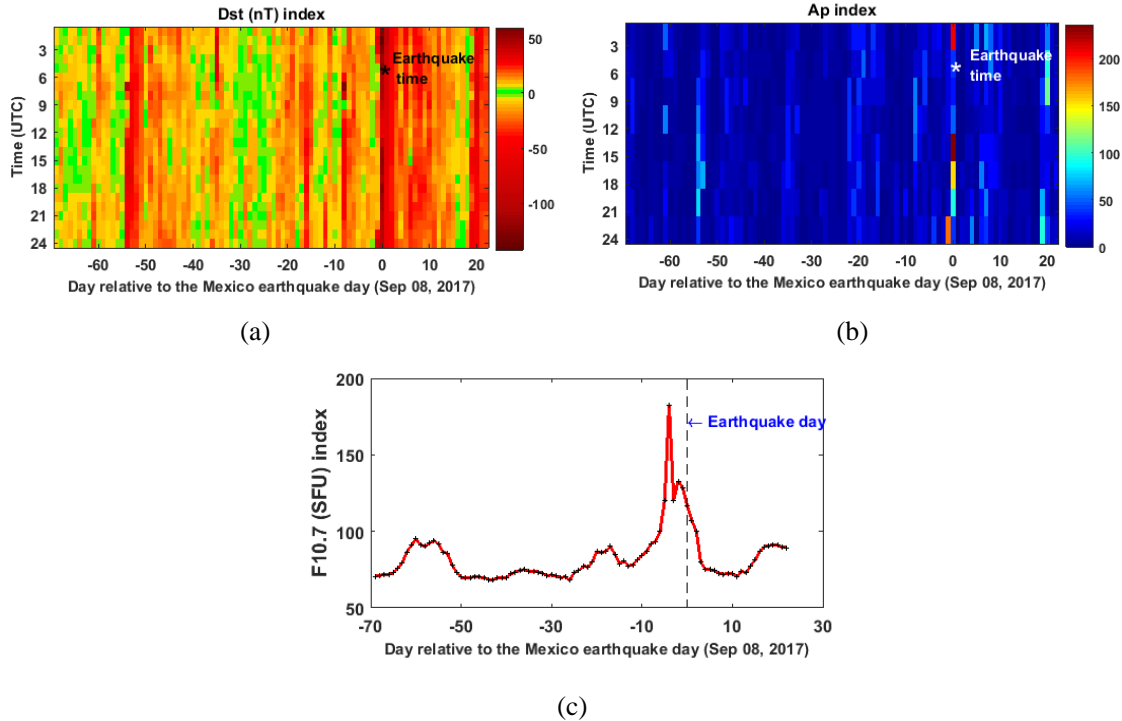
Figure 1. (a), (b) and (c) show, respectively, the variations of D_{st}, A_p, and solar radio flux (F10.7) indices during the period of July 1 to September 30, 2017. An asterisk indicates the earthquake time. The X-axis represents the days relative to the Mexico earthquake day.

(a)

(b)

(c)
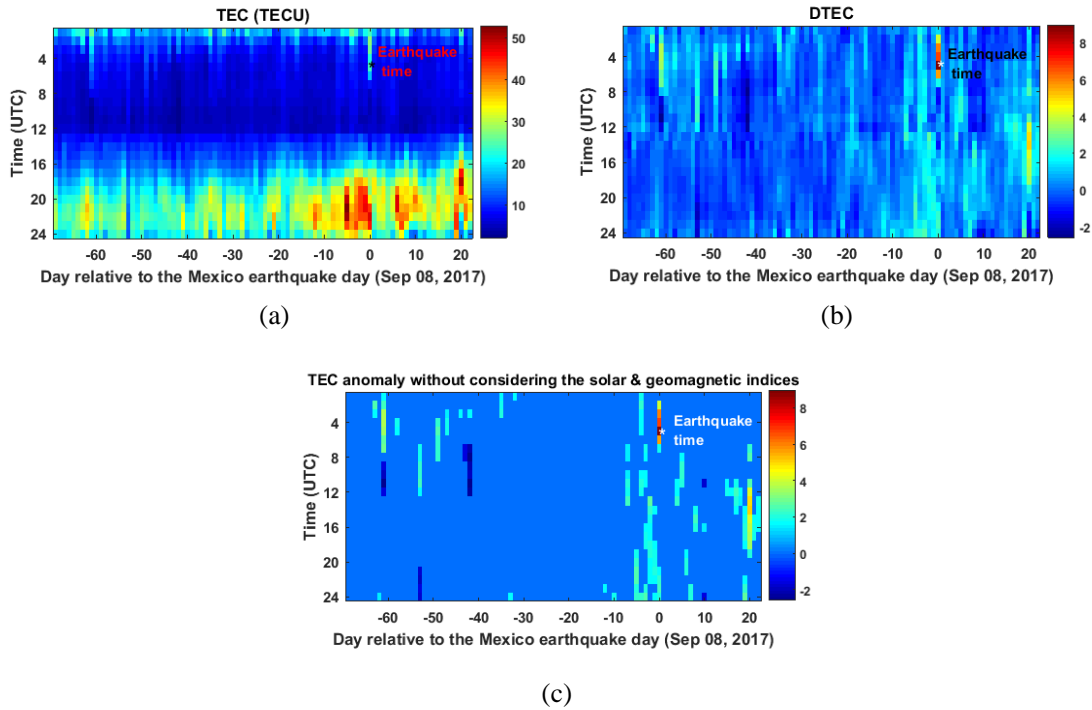
Figure 2. a) The variations of TEC, b) DTEC variations after implementing the median method and c) detected TEC anomalies using the median method when $|DTEC| > 1.5$.
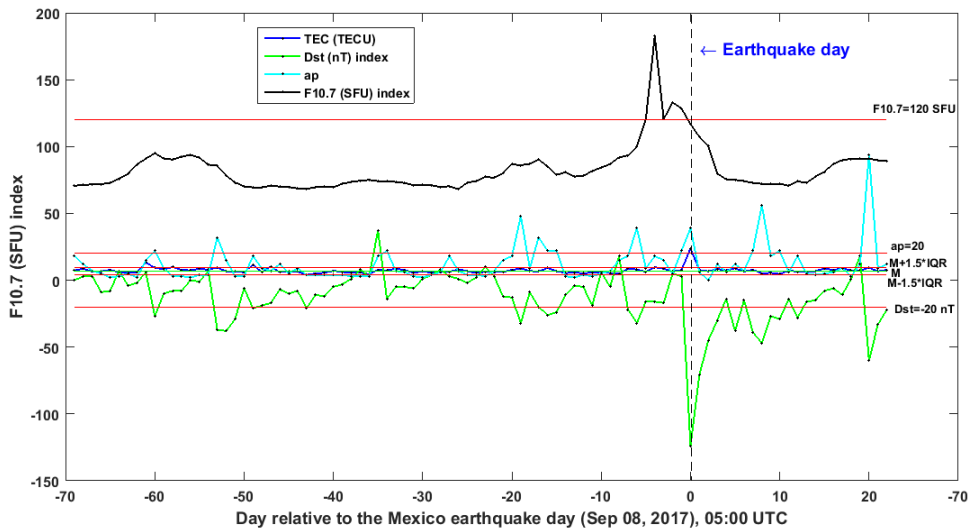
Figure 3. The time-series of variations of TEC, Dst, ap and F10.7 during the period of July 01 to September 30, 2017 at 05:00 UTC.

Figure 2(c) shows detected TEC anomalies using the median method when $|DTEC| > 1.5$ and without considering the non-quiet conditions of solar and geomagnetic activities. Liu et al. (2004) declared that if an observed TEC value falls out of either the associated lower or higher bound ($M\pm IQR$), it

can be concluded with a confidence level of about 80-85% that a lower or higher abnormal signal is detected. Therefore, based on the error ellipsoid theory, $M\pm1.5\times IQR$ bounds, increase the confidence level to about 90-95%.

There are a clump of clear anomalies around

the time of the earthquake. Then to distinguish pre-earthquake anomalies from the other anomalies related to the geomagnetic activities, the five conditions of $|DTEC| > 1.5$, Dst > -20 nt, Dst < 20 nt, Ap < 20 and F10.7 < 120, respectively, are jointly used using AND operator to construct the irregular variations map. It is seen that the all detected pre seismic anomalies in Figure 2(c) are masked by high geomagnetic activities. The detected anomalies on 25 and 26 September (17 and 18 days after the earthquake) could be associated with the after seismic events on 19 and 23 September (Table 1).

In order to implement the Kalman filter method, the half of the data has been used for training to obtain the optimum parameters. Figure 4(a) shows the differences between the predicted TEC values using the Kalman filter method and the observed TEC values during the 23 days before to 22 days after the earthquake. It is seen that these differences have reached the high values on five days

before the earthquake. Figure 4(b) shows the DTEC values obtained from $Dx = \dfrac{x - \mu}{\sigma}$, where μ and σ are the mean value and standard deviation of the differences values between the observed and the predicted values using a Kalman filter (x) at each hour, respectively. According to this, if the absolute value of Dx would be greater than k, ($|Dx| > k$), the behavior of the relevant parameter (x) is regarded as anomalous. Figure 4(b) illustrates striking anomalies between 2:00 and 5:00 UTC on earthquake day. Figure 4(c) shows detected TEC anomalies using the median method when $|DTEC| > 1$ and without the non-quiet conditions of solar and geomagnetic activities.

The unusual increase of TEC values clearly seen between 02:00 and 06:00 UTC, on earthquake day. It should be noted that the all detected pre seismic anomalies in Figure 4(c) are masked by high geomagnetic activities.

Table 1. Characteristics of the Mexico earthquake and its main aftershocks (reported by http://earthquake.usgs.gov/).

Date	Time (UTC)	Geographic Latitude, longitude	Magnitude (M_W)	Focal depth (km)
September 08, 2017	04:49:19	15.022° N, 93.899° W	8.2	47.40
September 19, 2017	18:14:38	18.568° N, 98.481° W	7.1	51.0
September 23, 2017	12:53:02	16.773° N, 94.951° W	6.1	9.6

(a)

(b)

(c)
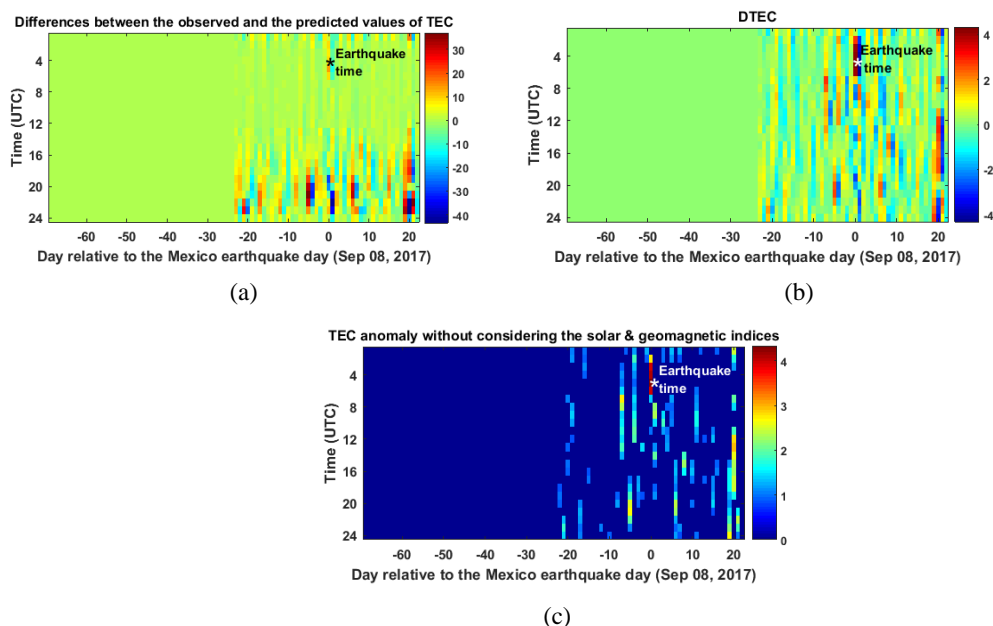
Figure 4. a) Differences between the observed and the predicted values of TEC obtained using the Kalman filter method. b) DTEC variations. c) Detected anomalies using a Kalman filter method without considering the non-quiet conditions of solar and geomagnetic activities.

To implement the NN method, half of the data were selected as training data. Using the training data, the network parameters are determined and then based on the constructed pattern vectors in feature space the prediction process is done. In the case of a testing process, if the difference value PE_I between the observed value X_i and the predicted value $\hat{X}_i$, is outside the pre-defined bounds $\mu \pm 2.0 \times \sigma$, ($\mu$ and σ are the mean and the standard deviation of PE_i values) the irregular variation is detected.

Figure 5(a) is a representation of the differences in values between the observed and the predicted values during the testing set. Sharp anomalies are seen on earthquake day. Figure 5(b) shows the DTEC values obtained from $Dx = \dfrac{x - \mu}{\sigma}$, where μ, σ are the mean and standard deviation of differences in values (x) at each hour, respectively. In Figure 5(c), anomalous TEC values are only depicted at times when $|DTEC| > 1$. Then, to distinguish pre-earthquake anomalies from the other anomalies related to the geomagnetic activities, the five conditions of $|DTEC| > 1$, Dst > -20 nt, Dst < 20 nt, Ap < 20 and F10.7 <120, are jointly used using AND operator to construct the irregular variation map. However, the all detected pre seismic anomalies in Figure 5(c) are masked by high geomagnetic activities.

5-5. Discussion and Conclusions

So far, different hypotheses about the behavior of earthquake precursors have been raised based on geophysical and geochemical processes. However, none of them have been accepted (Qiang et al., 1991; Freund, 2009; Pulinets and Ouzounov, 2011). One way to justify the behavior of earthquake precursors can be multi-precursors analysis that attempts to detect anomalous variations in different layers of lithosphere, atmosphere and ionosphere and justify their relationship with each other (Akhoondzadeh, 2011; Akhoondzadeh et al., 2018).

(a)

(b)

(c)
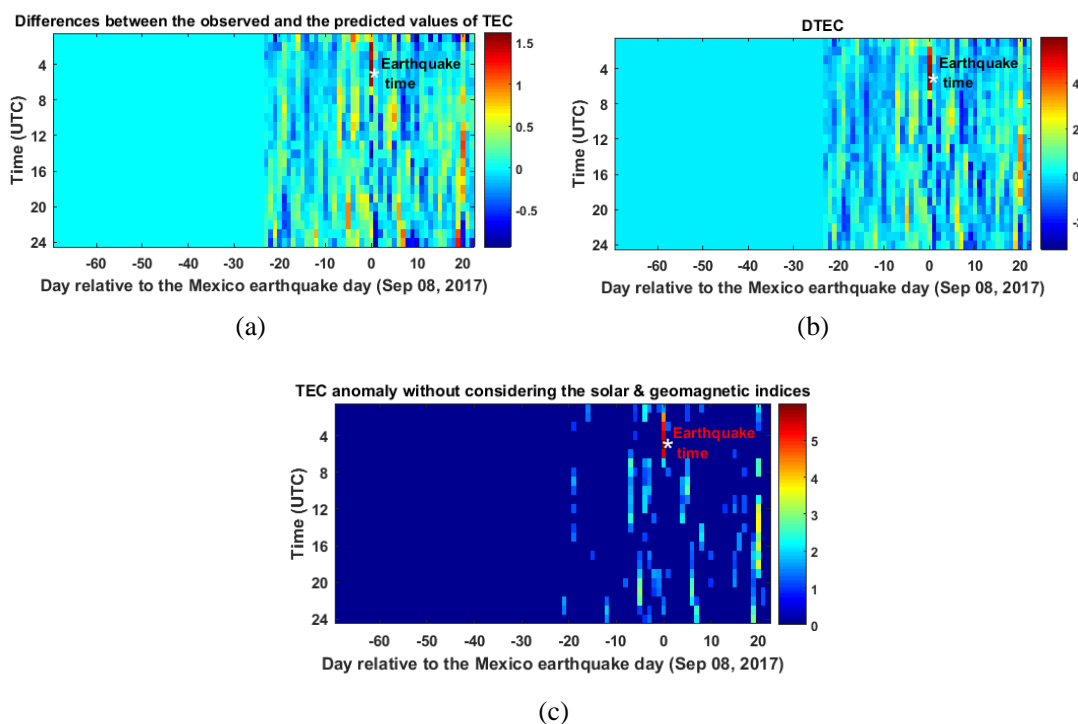
Figure 5. a) Differences between the observed and the predicted values of TEC obtained using the NN method. b) DTEC variations. c) Detected anomalies using the NN method without considering the geomagnetic indices.

In this study, three standard, classical and intelligent algorithms including median, Kalman filter, and NN, respectively were implemented for detection of irregular variations around the time of the Mexico (M_w=8.2) earthquake of September 08, 2017. Every three methods detect very striking irregular variations on earthquake day. However, solar- geomagnetic parameters indicate higher activities on earthquake day. Therefore, there is ambiguity about the association of these TEC irregular variations with seismic activity as a mixed and complex behavior of the ionosphere is encountered. It is necessary to take into account that the ionosphere has a complicated behavior even under the quiet geomagnetic condition and the measured parameters sometimes display variations in a quiet seismic condition that can be associated with other unknown factors. The existence of a dense distribution of GPS stations in most parts of the world and the continuous monitoring of TEC may help to create an effective earthquake warning system. One of the most important advantages of using learning methods such as NN is that the prediction process is improved according to the size of the training data. Of course, it should be noted that the impacts of other factors such as solar-geomagnetic activities at least about ionospheric precursors, should be considered.

Acknowledgement

References

Akhoondzadeh, M., 2011, Comparative study of the earthquake precursors obtained from satellite data. PhD thesis, University of Tehran, Surveying and Geomatics Engineering Department, Remote Sensing Division.

Akhoondzadeh, M., 2012, Anomalous TEC variations associated with the powerful Tohoku earthquake of 11 March 2011. Nat. Hazards Earth Syst. Sci., 12, 1453-1462, doi:10.5194/nhess-12-1453-2012.

Akhoondzadeh, M., 2013, A MLP neural network as an investigator of TEC time series to detect seismo-ionospheric anomalies. Advances in Space Research, 51, 2048-2057.

Akhoondzadeh, M., De Santis, A., Marchetti, D., Piscini, A. and Cianchini, G., 2018, Multi precursors analysis associated with the powerful Ecuador (MW=7.8) earthquake of 16 April 2016 using Swarm satellites data in conjunction with other multi-platform satellite and ground data. Advances in Space Research, 61, 248-263.

Freund, F., 2009, Stress-activated positive hole charge carriers in rocks and the generation of pre-earthquake signals. In Electromagnetic phenomena associated with earthquakes, Ed. by M. Hayakawa, Transworld Research Network, Trivandrum, 41-96.

Hayakawa, M. and Molchanov, O. A., 2002, Seismo- Electromagnetics: Lithosphere-Atmosphere-Ionosphere Coupling. Terra Scientific Publishing Co. Tokyo, 477.

Haykin, S., 2001, Kalman filtering and Neural networks, John Wiley & Sons, Inc, McMaster University, Hamilton, Canada, 1-284.

Klimenko, M. V., Klimenko, V. V., Zakharenkova, I. E. and Pulinets, S. A., 2012, Variations of equatorial electrojet as possible seismo-ionospheric precursor at the occurrence of TEC anomalies before strong earthquake, Advances in Space Research, 49 (3), 509-517.

Liu, J. Y., Chuo, Y. J., Shan, S. J., Tsai, Y. B., Pulinets, S. A. and Yu, S. B., 2004, Pre-earthquake-ionospheric anomalies registered by continuous GPS TEC, Ann. Geophys., 22, 1585-1593.

Mannucci, A. J., Wilson, B. D., Yuan, D. N., Ho, C. H., Lindqwister, U. J. and Runge, T. F., 1998, A global mapping technique for GPS-derived ionospheric total electron content measurements, Radio Sci., 33, 565-582, doi: 10.1029/97RS02707.

Mayaud, P. N., 1980, Derivation, Meaning and use of geomagnetic indices, Geophy, 22, American Geo. Union, Washington, D. C.

Namgaladze, A. A., Zolotov, O. V. and Prokhorov, B. E., 2013, Numerical

Simulation of the Variations in the Total Electron Content of the Ionosphere Observed before the Haiti Earthquake of January 12, 2010, Geomagnetism and Aeronomy, 53 (4), 553-560.

Pao, H. T, 2007, Forecasting electricity market pricing using artificial neural networks, Energy Conversion and Management, 48, 907–912.

Paoli, C., Voyant, C., Muselli, M. and Nivet, M. L., 2010, Forecasting of preprocessed daily solar radiation time series using neural networks, Solar Energy, 84, 2146–2160.

Parrot, M., 1995, Use of satellites to detect seismo-electromagnetic effects, Main phenomenological features of ionospheric precursors of strong earthquakes, Advances in Space Research, 15 (11), 1337-1347.

Pulinets, S. A. and Boyarchuk, K. A., 2004, Ionospheric Precursors of Earthquakes, Springer, Berlin.

Pulinets S. A., 2009, Physical mechanism of the vertical electric field generation over active tectonic faults, Adv. Space Res., 44, 767-773.

Pulinets S. and Ouzounov D., 2011, Lithosphere-Atmosphere-Ionosphere Coupling (LAIC) model - an unified concept for earthquake precursors validation, Journal of Asian Earth Sciences, 41, 371-382.

Qiang, Z. J., Xu, X. D. and Dian, C. G., 1991, Thermal infrared irregular variation precursor of impending earthquakes, Chinese Sciences Bulletin, 36, 319-323.

Sorokin, V. M. and Pokhotelov, O.A., 2014, Model for the VLF/LF radio signal anomalies formation associated with earthquakes, Advances in Space Research, 54 (12), 2532-2539.

Zhang, G. P., 2001, An investigation of neural networks for linear time-series forecasting, Computers & Operations Research, 28, 1183-1202.